Large-deformation analysis of pile installation with subsequent lateral loading: Sanisand vs. Hypoplasticity

Patrick Staubach[i)]; Jan Machaček[ii)]; Torsten Wichtmann[iii)];

Abstract: The simulation of the installation of open-ended piles using a Coupled Eulerian-Lagrangian method in conjunction with two sophisticated constitutive soil models, Sanisand and Hypoplasticity with intergranular strain extension, is presented. Insights into the requirements of numerically stable and efficient implementations of the constitutive models are provided. Following its installation, the response of the pile to lateral loading is investigated and the numerical results are compared to results of model tests. Sanisand is found to be superior in terms of computational performance for the simulation of the pile installation but predicts the pile response to lateral loading following the installation process worse compared to the simulations using Hypoplasticity. The installation-induced changes in the soil state have less influence on the lateral pile response in case of the simulations using Sanisand. It is concluded that both constitutive models are suitable to study large-deformation pile installation processes but the results can differ significantly between the constitutive models despite a careful calibration of the material constants.

Keywords: Pile driving, Large-deformation, Sanisand, Hypoplasticity, Coupled Eulerian-Lagrangian, Lateral loading

1 Introduction

The simulation of the installation of piles is a topic of great interest in the geotechnical community. The rapid improvement of computational resources and methods over the last decade has enabled to perform simulations of large-deformation processes such as pile driving using sophisticated constitutive soil models, which are able to reproduce many aspects of the mechanical behaviour of soils.

From experimental [12, 26, 14, 3, 2, 22] and numerical investigations [20, 13, 52, 51] it is known that the pile installation process in sandy soils does not only influence the vertical load-displacement response of the pile once in service, but also the response to horizontal loading. To simulate the lateral loading response of driven piles realistically, the incorporation of the installation-induced soil changes around the pile is thus judged to be of great importance.

In a preceding work [50] a back-analysis of small-scale model tests on piles subjected to lateral loading by Leblanc et al. [30] was performed. The pile installation process prior to the lateral loading has been taken into account and the lateral response of the pile has been investigated for simulations with and without consideration of the installation process, respectively. For these simulations Hypoplasticity with intergranular strain extension (for sake of convenience referred to as the *hypoplastic model* or *Hypoplasticity* in the following) has been utilized as constitutive model for the simulation of the installation process as well as for the lateral loading of the pile following its installation. The installation process was found to result in a stiffer response of the pile when subjected to lateral loading and a better accordance with the experimental values was observed when considering the installation process in the numerical simulations.

Most numerical investigations on pile installation have either employed hypoplastic models [17, 15, 11, 43, 48, 18, 45, 20, 16, 10, 1, 27, 21, 29] or simple elasto-plastic models [4, 23, 60, 1]. Despite being a frequently applied constitutive model and being constantly extended (see e.g. [28, 9, 32, 33, 59, 42]), the Sanisand constitutive model has yet not been applied for the simulation of large-deformation pile installation. In this work, the model tests of Leblanc et al. [30] are simulated using the Sanisand constitutive model

[i)] Chair of Geotechnics, Bauhaus Universität Weimar, Germany/Chair of Soil Mechanics, Foundation Engineering and Environmental Geotechnics, Ruhr Universität Bochum, Germany. Email: patrick.staubach@uni-weimar.de, Corresponding author.

[ii)] Institute of Geotechnics, Technische Universität Darmstadt, Germany/Chair of Soil Mechanics, Foundation Engineering and Environmental Geotechnics, Ruhr-Universität Bochum, Germany

[iii)] Chair of Soil Mechanics, Foundation Engineering and Environmental Geotechnics, Ruhr-Universität Bochum, Germany

(version of 2004, see [8]) as well as Hypoplasticity with intergranular strain extension. The aim of this study is to investigate the influence of the constitutive model on the predicted soil behaviour during the pile installation using the Coupled Eulerian-Lagrangian (CEL) method as well as the influence of the constitutive model on the lateral loading response following the pile installation process. In order to ensure the correct representation of the constitutive soil behaviour, the material constants of Sanisand as well as Hypoplasticity are determined based on data from oedometric compression tests as well as drained monotonic triaxial tests performed on yellow Leighton-Buzzard sand used in the experiments by [30].

The paper is structured as follows: Some aspects of the implementation of the constitutive models are discussed in Section 2. In Section 3 the small-scale model tests on piles subjected to lateral loading performed by [30] are introduced. The determination of the constitutive model parameters is described in Section 4. The simulation of the pile installation process prior to the lateral loading is presented in Section 5. Following its installation, the response of the pile to lateral loading is investigated in Section 6.

2 Implementation of the constitutive models

Both constitutive models, Hypoplasticity with intergranular strain extension (see [58] and [40]) and Sanisand (see [8]), are implemented as `VUMAT` subroutines offered by the commercial software `Abaqus` for the incorporation of user-defined material models in explicit analyses. Because the material undergoes large deformations during the pile penetration process, the numerical stability of the implementations is of great importance.

2.1 Additional viscous stress

An additional viscous stress increment $\Delta\boldsymbol{\sigma}^{\text{vis}}$, which depends on the mean effective stress p (positive values indicate pressure) and increases with p approaching zero, is added to the increment of the constitutive stress $\Delta\boldsymbol{\sigma}^{\text{c}}$:

$$\Delta\boldsymbol{\sigma} = \Delta\boldsymbol{\sigma}^{c} + \Delta\boldsymbol{\sigma}^{\text{vis}}. \tag{1}$$

$\Delta\boldsymbol{\sigma}^{\text{vis}}$ is not considered on the material level of the calculation since it is subtracted from the stress which is used for the call of the material model in the following increment. Thus, the viscous stress does not directly alter the material response but adds damping to the model. The additional damping reduces the stable time increment used in the global explicit integration scheme (and therefore more increments are needed) but enhances the numerical stability.

The viscous stress is calculated using $\Delta\boldsymbol{\sigma}^{\text{vis}} = \lambda\mathbf{1}\text{tr}(\Delta\boldsymbol{\varepsilon}) + 2\mu\Delta\boldsymbol{\varepsilon}$, where λ and μ are functions of the mean effective stress p. $\lambda = \mu$ is set for the present simulations. λ is calculated using:

$$\lambda = \begin{cases} 0.04 \text{ kPas} & \text{for } p > 0.2 \text{ kPa} \\ 0.04 \text{ kPas} + 0.1 \text{ kPas}\left(1 - \dfrac{p}{0.2 \text{ kPa}}\right) & \text{for } p < 0.2 \text{ kPa}. \end{cases}$$

The additional viscous stress is utilized for the simulations with both constitutive models.

2.2 Return-mapping algorithm

In case of the hypoplastic model, no return-mapping algorithm is necessary, since no yield surface exists. Therefore, the constitutive model can technically not diverge on the integration point level (however, depending on the implementation, some error control might be exceeded, which then results in non-convergence). In case of Sanisand, stress states violating the yield criterion have to be mapped back on the yield surface using a return-mapping algorithm. The yield criterion used in Sanisand is defined by (see [8]):

$$f = \left[(\mathbf{s} - p\boldsymbol{\alpha}) : (\mathbf{s} - p\boldsymbol{\alpha})\right]^{\frac{1}{2}} - \sqrt{\frac{2}{3}}pm \tag{2}$$

$\boldsymbol{\alpha}$ is the back-stress tensor and a state variable of Sanisand. $\mathbf{s}$ is the stress deviator and m is a material parameter determining the elastic range of the model. Setting $\mathbf{s} = p\boldsymbol{\alpha}$ the current state is in the centre of the yield locus.

In most cases, rapid convergence of the return-mapping algorithm is achieved. For some stress states, however, the return-mapping algorithm may diverge. Since it is neither desirable that the calculation is aborted in such a case nor that the simulation continues with an un-satisfied yield criterion, a rigorous correction of the back-stress tensor $\boldsymbol{\alpha}$ is made. For a given stress state, the yield surface is exactly satisfied, i.e. the stress state is on the yield locus, in case of:

$$\boldsymbol{\alpha} = \frac{\mathbf{s}}{p} - \mathbf{n}\sqrt{\frac{2}{3}}m \tag{3}$$

with $\mathbf{n}$ being defined by:

$$\mathbf{n} = (\mathbf{s} - p\boldsymbol{\alpha})^{\rightarrow}. \tag{4}$$

In Eq. (4) the definition $(\sqcup)^{\rightarrow} = \sqcup/\|\sqcup\|$ holds. Using $\mathbf{n} : \mathbf{n} = 1$ it is evident that f in Eq. (2) is zero when setting $\boldsymbol{\alpha}$ according to Eq. (3). Of course, this artificial adjustment of the back-stress tensor $\boldsymbol{\alpha}$ influences the material response and it has to be secured that it is performed only rarely. During the simulation of the pile driving process it has thus been checked that the correction of the back-stress tensor is only applied for elements undergoing the most severe deformations (e.g. below the tip of the pile).

2.3 Small mean effective stresses and integration of the stress rate

Since in case of vanishing mean effective stress the material response is not defined or becomes unstable. In these cases, a correction for small mean effective stresses ($p < 0.01$ kPa) and a subsequent correction of stress states located outside of the Matsouka-Nakai failure locus is made for both constitutive models. The Matsouka-Nakai failure locus is defined by [39]

$$F = -\frac{I_1 I_2}{I_3} - 9 - 8\tan^2(\varphi) \leq 0, \tag{5}$$

where the principal invariants I_1, I_2, I_3 of the stress tensor are used. The projection on the Matsouka-Nakai failure locus has been proposed in [41] and has been also used successfully for the simulation of liquefiable soils during earthquake loading and vibratory pile driving in water-saturated sand [37, 49].

Both constitutive models are implemented using an explicit sub-stepping scheme to integrate the constitutive equations. In case of the implementation of the hypoplastic model, an adaptive explicit Euler scheme to integrate the stress rate within a sub-stepping method with error control (see [47]) is employed. The error of the explicit scheme within every sub-increment is calculated and the size of the sub-increment is reduced if the error is too large. Likewise, the sub-increment size is increased if the error is small. In case of Sanisand, a simpler sub-stepping scheme without error control and constant sub-increment size is used.

Since the volumetric strain during the pile installation process can be extremely large for some elements, the void ratio can reach values smaller or larger than the minimum and maximum void ratio, respectively. In order to prevent any un-physical response of the constitutive models in this case, the void ratio is restricted to a minimum of $0.9 \cdot e_{\min}$ and a maximum of $1.1 \cdot e_{\max}$. Note that these fractions are assumptions and are chosen based on experience.

Both constitutive models have been newly implemented with the aim to secure numerical stability even for strongly non-linear boundary value problems with large deformations such as pile driving. The implementations have been used in [36] for the simulation of vibratory pile driving in water-saturated sand as well. Other, publicly available implementations of the two constitutive models were found not to be numerically stable for the simulation of pile installation. The implementation of both constitutive models as `VUMAT` subroutines suitable for `Abaqus` is available from the first author upon request.

3 Small-scale model tests by Leblanc et al.

The geometric specifications of the model tests performed by Leblanc et al. [30] as well as a photo of the device are given in Fig. 1. The copper pile (diameter $D = 0.08$ m, wall thickness $t = 0.002$ m) has been driven into the soil using a plastic hammer until an embedment length of $L = 0.36$ m had been reached. In relation to a typical monopile foundation for offshore wind power plants, a scaling of the monopile dimensions of 1:50 has been applied. Dry yellow Leighton-Buzzard sand has been used. It was poured into the container from a low drop height in order to achieve a loose initial state of the soil prior to the pile installation. The test considered for the back-analysis had an initial relative density of $D_{r0} = 38\%$. According to Leblanc et al. [30], the peak friction angle for the given stress conditions and relative density of the small-scale model tests is equivalent to the peak friction angle of the same soil at a relative density of $D_{r0} = 75\%$ and an acting effective stress being representative for the real-scale model. The lateral loading of the pile following its installation has been applied in a height of $e = 0.43$ m above the ground surface.

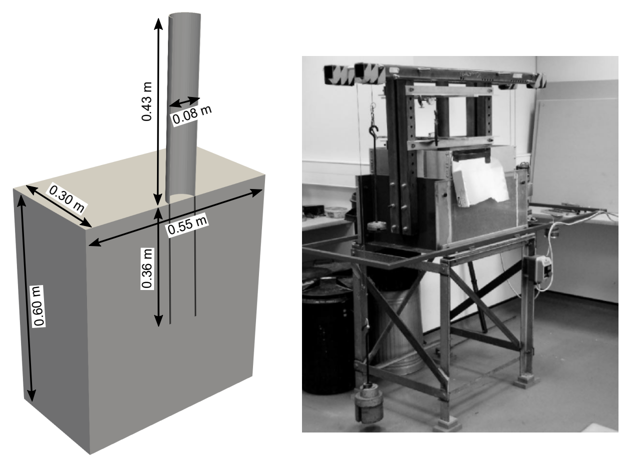

Fig. 1: Dimensions of the model test and picture of the device (reprinted from [30])

4 Determination of the constitutive parameters for Leighton-Buzzard sand

In order to determine the constitutive model parameters for yellow Leighton-Buzzard sand (LBS), oedometric compression and drained monotonic triaxial tests have been performed. The calibration of the parameters for the hypoplastic model has already been documented in [50]. Therefore, the focus is on the calibration of the Sanisand model in the following. Note that all laboratory tests have been simulated using the same set of parameters for a certain constitutive model, given in Table 1 for the hypoplastic model and in Table 2 for Sanisand. A better agreement between simulations and experiments could have been achieved

φ_c	e_{i0}	e_{c0}	e_{d0}	h_s	n	α
33.3°	0.930	0.809	0.507	$1.9 \cdot 10^7$ kPa	0.191	0.223

β	R	m_R	m_T	β_R	χ
-1.3	10^{-4}	4	2	0.1	4.6

Table 1: Parameters of Hypoplasticity with intergranular strain extension for yellow Leighton-Buzzard sand

p_a	e_0	λ_c	ξ	M_c	M_e	m	G_0
100 kPa	0.87	0.12	0.2	1.34	0.94	0.05	50

ν	h_0	c_h	n_b	A_0	n_d	$z_{\max}$	c_z
0.05	10	0.75	1.2	0.6	2	20	10000

Table 2: Parameters of *Sanisand* for yellow Leighton-Buzzard sand

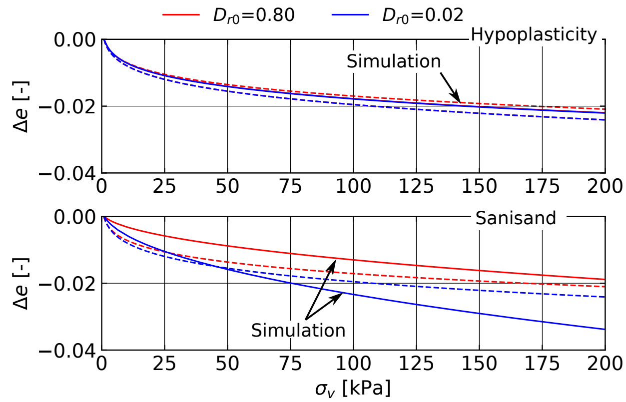

Fig. 2: Results of two oedometric compression tests with different initial relative densities ($D_r = 0.80$ and $D_r = 0.02$) and the simulations using the hypoplastic model and Sanisand, respectively. The parameters given in Table 1 and 2 have been used.

if an individual set of parameters would have been calibrated for each type of laboratory test. In order to achieve meaningful comparisons of the two constitutive models for the pile installation simulations, the calibration of Sanisand has been performed with the aim to fit to the results of the hypoplastic model as well as to the laboratory data. Initially, the parameters of Sanisand have been set identical to the parameters determined in [57] for a similar sand ("Karlsruhe fine sand"), before they were adjusted to fit better to the laboratory data for LBS.

The simulation of two oedometric compression tests with different initial relative densities ($D_r = 0.80$ and $D_r = 0.02$) is displayed in Fig. 2. The change in void ratio Δe with increasing vertical stress σ_v is given for the simulation with the hypoplastic model and Sanisand, respectively. The simulation using the hypoplastic model shows a good agreement for both tests. Only little influence of the initial density on Δe is found. Using the Sanisand model, the change in void ratio is predicted too small in case of the dense sample but too large for the initially loose sample. However, the influence of the initial density on Δe is qualitatively correctly predicted by Sanisand. Note that the elastic material parameters G_0 and ν have to be set to very small values in order to achieve acceptable results using Sanisand. Similar conclusions have been drawn in [57, 36] for the simulation of oedometric compression tests. It is expected that the low value for G_0 in the present case leads to a worse approximation of the soil response at small strain. This could be investigated utilizing additional data from cyclic triaxial tests. For the time being, however, the value determined based on the oedometric tests is used. Note that some of these issues could be resolved using the Sanisand version of 2008 [54], which is able to account for plastic strain without a change in stress ratio and is hence able to better capture the soil response under oedometric compression.

The simulations of two drained monotonic triaxial tests with differing initial relative density ($D_{r0} = 0.54$ and $D_{r0} = 0.18$) but identical initial mean effective stress of $p_0 = 20$ kPa are given in Fig. 3. Note that the initial stress level has been intentionally chosen low in order to best represent the stress conditions in the small-scale model tests of Leblanc et al. The simulation using the hypoplastic model predicts too low residual values of the deviatoric stress q at large strains and underestimates the dilatancy. Likewise, the residual values of q as well as the volumetric strain are underestimated using the Sanisand model. The dilatancy could be increased by increasing the parameter A_0. However, since a good fit with the results of the hypoplastic model is targeted as well and the intensity of dilatancy in the hypoplastic model can not directly be controlled with a parameter without changing the q-ε_{11} curve, the slight deviation from the experimental results is accepted. In case of the initially medium dense sample, the hypoplastic model predicts a much larger peak in the q-ε_{11} curve compared to Sanisand. The parameter n_b of Sanisand, controlling the peak of the q-ε_{11} curve, could be increased to reach a higher peak friction angle. However, the q-ε_{11} curve of the initially loose sample would then not fit as well to the results of the hypoplastic model.

Since the stress increases significantly below the pile tip during the pile installation process, an adequate response of the constitutive models for higher stresses has to be secured as well. Therefore, the results of a second series of drained monotonic triaxial tests with initial relative densities ($D_{r0} = 0.46$ and $D_{r0} = 0.17$) similar to the first two tests but higher initial mean effective stress ($p_0 = 50$ kPa) are given in Fig. 4. Compared to the tests with $p_0 = 20$ kPa, the predicted peak and residual values of q are in better accordance with the experimental values for both constitutive models. For the initially medium dense sample, the hypoplastic model predicts a larger peak of the q-ε_{11} curve compared to the simulation using Sanisand similar to the test with $p_0 = 20$ kPa. The ε_{vol}-ε_{11} curves are well reproduced by both constitutive models.

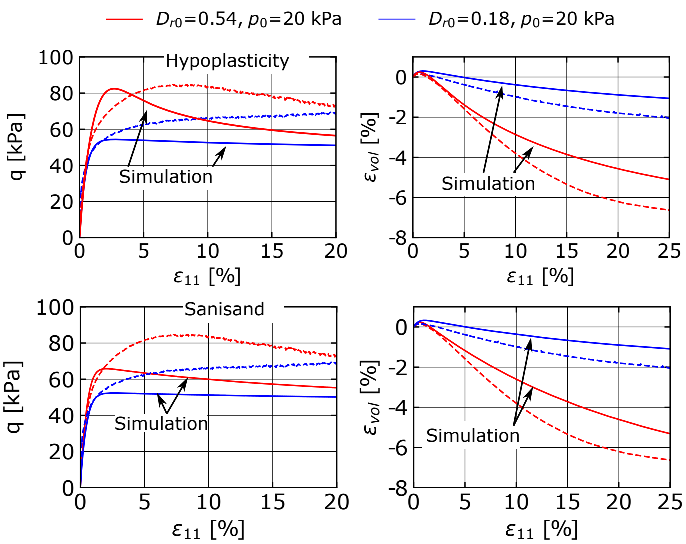

Fig. 3: Results of two drained monotonic triaxial tests with varying initial densities and an initial mean effective stress of $p_0 = 20$ kPa and the simulations using the hypoplastic model and Sanisand, respectively. The parameters given in Table 1 and 2 have been used.

5 Numerical model and results for the pile installation process

5.1 Numerical model

The installation of the pile is simulated using a Coupled Eulerian-Lagrangian (CEL) method, where the soil is modelled using Eulerian elements and the pile is considered as Lagrangian body. The CEL method has proven a suitable numerical method for the simulation of soil undergoing large deformations while being in contact with a more rigidly behaving body (see [46, 19, 55, 53]). It is worth noting that recent investigations on the pile installation process using the discrete element method (DEM) show promising results as well [31, 34].

The CEL model used for the simulation of the installation process is displayed in Fig. 5a). The red volume is initially empty of soil material but could be filled if the soil heaves during the driving process. The blue volume is initially fully material filled and has dimensions identical to the sand volume in the container used in the experiment displayed in Fig. 1. Exploiting the symmetry in case of the pile installation, a quarter model is considered for the simulation to reduce the computational costs. Note that no axisymmetric simulation is possible due to restrictions of the utilized software. The boundary conditions of the experiment are adopted and no friction at the borders of the sand container is accounted for, i.e. vertical roller supports at the bottom of the model and horizontal roller supports normal to the model border at the vertical sides are defined. As in the model test, a homogeneously distributed initial relative density of 38 % is assumed. Friction between pile and soil is considered using a Coulomb friction model. The wall friction angle is set to be 2/3 of the critical friction angle, which is an assumption since no detailed information on the surface roughness of the pile is available.

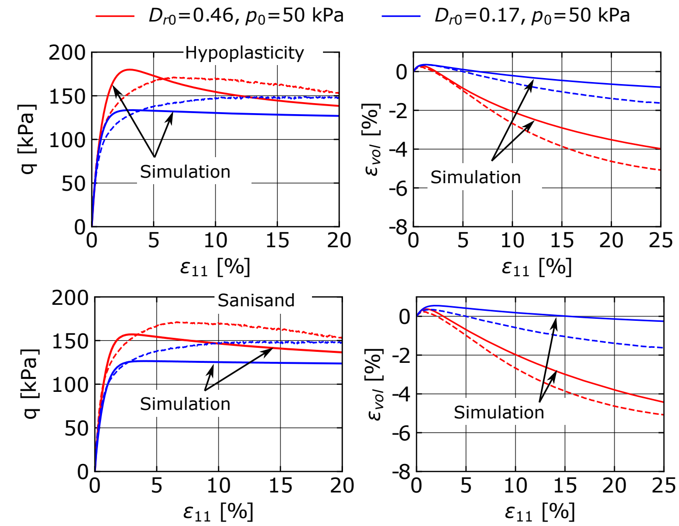

Fig. 4: Results of two drained monotonic triaxial tests with varying initial densities and an initial mean effective stress of $p_0 = 50$ kPa and the simulations using the hypoplastic model and Sanisand, respectively. The parameters given in Table 1 and 2 have been used.

Despite being impact driven with a plastic hammer in the model tests, the pile is jacked into the soil with an assumed velocity of 0.06 m/s in the simulations. This is due to the unknown specifications of the impact force as well as the larger number of hammer strokes applied in the experiment (approximately 700). Since the time required to apply the strokes is large, a numerical simulation of all individual strokes is not possible with computational resources available. In order to investigate how strongly the installation technique (jacking vs. impact driving) influences the results of the simulations, the impact driving has been partly simulated and compared to the jacked pile in [50]. It was found that the installation-induced changes in the soil in the vicinity of the pile were not strongly altered using impact driving compared to jacking. The response of the pile to lateral loading following the installation was also not strongly influenced by the installation technique. Findings from recently performed field tests support this observation

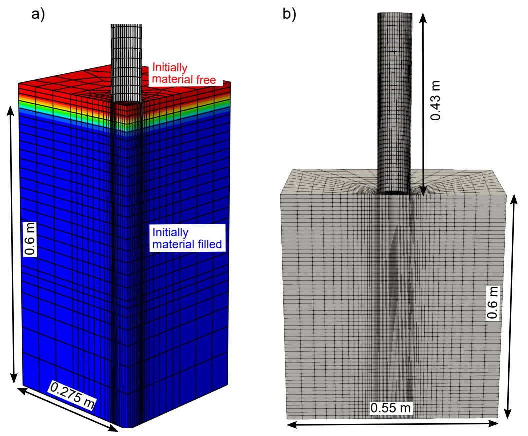

Fig. 5: a) Finite element model used for the CEL analysis (Abaqus) and b) Purely Lagrangian finite element model used for the lateral loading of the pile following its installation (`numgeo`)

[3]. Opposite to that, centrifuge tests comparing impact driven with jacked piles showed a higher lateral resistance for the impact driven piles [14]. The differences in these findings are likely to be caused by the differences in pile geometry, initial soil state and specifications of the applied installation technique.

The CEL method is implemented in an explicit time integration scheme. No time scaling factor for the critical time increment of the explicit time integration scheme is applied. Note that no effects due of grain crushing are incorporated in the simulations. Due to the high stresses during the process it is expected that grain crushing will influence the results to some extend. Future work could focus on the investigation of the influence of grain grushing using the constitutive models proposed e.g. in [7, 44]. A calibration with additional laboratory tests with high stress level to trigger grain crushing effects should then be performed in addition.

5.2 Results of the pile driving process

In order to evaluate if the soil prior to the pile driving process is considered loose or dense, the critical void ratio is calculated. Using the empirical relation for the critical void ratio employed by the hypoplastic model and proposed by Bauer [5]

$$e_c = e_{c0} \cdot e^{-(3p/h_s)^n}, \tag{6}$$

where e_{c0} is the critical void ratio at a mean effective stress of $p = 0$ kPa and h_s and n are the material constants for LBS given in Table 1, $e_c(p = 2 \text{ kPa}) \approx 0.764$ is calculated. Since the initial void ratio prior to the driving is $e_0 = 0.694$, the soil is considered dense and behaves dilatant during shearing.

Fig. 6 displays the spatial distribution of the relative density at different stages of the pile penetration process using the hypoplastic model and Sanisand, respectively. For a penetration of $t = 6$ cm both constitutive models predict a decrease in relative density at the ground surface in the vicinity to the pile. In case of the hypoplastic model an increase in relative density below the pile tip is evident, which is not the case using Sanisand. The simulation using Sanisand shows an increase in relative density in the symmetry axis of the model in greater soil depths. With ongoing pile penetration, a compaction of the soil inside and outside the pile in the vicinity of the pile shaft is observed in case of the simulation using the hypoplastic model. Until $t = 32$ cm no such compaction in the vicinity of the pile tip is visible using Sanisand. From the development of relative density over time it is, however, to be expected that with further pile penetration, such a compaction zone would develop in the simulation using Sanisand as well. In the soil surrounding the pile head close to the ground surface a strong loosening of soil is observed for both constitutive models, with the simulation using the hypoplastic model showing a much larger radius of soil with decreased density.

Opposite to the hypoplastic model, the simulation using Sanisand shows large settlement of the soil column inside of the pile, which can be traced back to greater compaction of the soil close to the symmetry axis of the model and less dilatancy of the soil close to the ground surface compared to the simulation using the hypoplastic model. Overall it can be noted that during the penetration process using Sanisand less dilatancy of the soil occurs close to the ground surface but more compaction in the soil close to the symmetry axis.

The spatial distribution of mean effective stress during the penetration process is displayed in Fig. 7. For $t = 6$ cm the simulation using the hypoplastic model predicts very high stresses below the pile tip whereas in case of Sanisand the stress is more concentrated in the soil close to the symmetry axis of the model. This observation is in accordance with the distribution in relative density discussed earlier, where a greater reduction of the void ratio close to the symmetry axis using Sanisand is observed. After a pile penetration of $t = 32$ cm both constitutive models predict high mean effective stresses below the pile reaching up to the bottom of the model. In case of the simulation using Sanisand a cone-shaped distribution is observed whereas the hypoplastic model shows more of a vertical streak of mean effective stresses larger than 100 kPa.

Fig. 8 displays the spatial distribution of radial stress after a penetration of 25 cm and 30 cm, respectively. The results of the hypoplastic simulation are displayed. The plots below show the radial stress distribution with respect to the radial distance to the pile. Both plots have been evaluated 25 cm below the

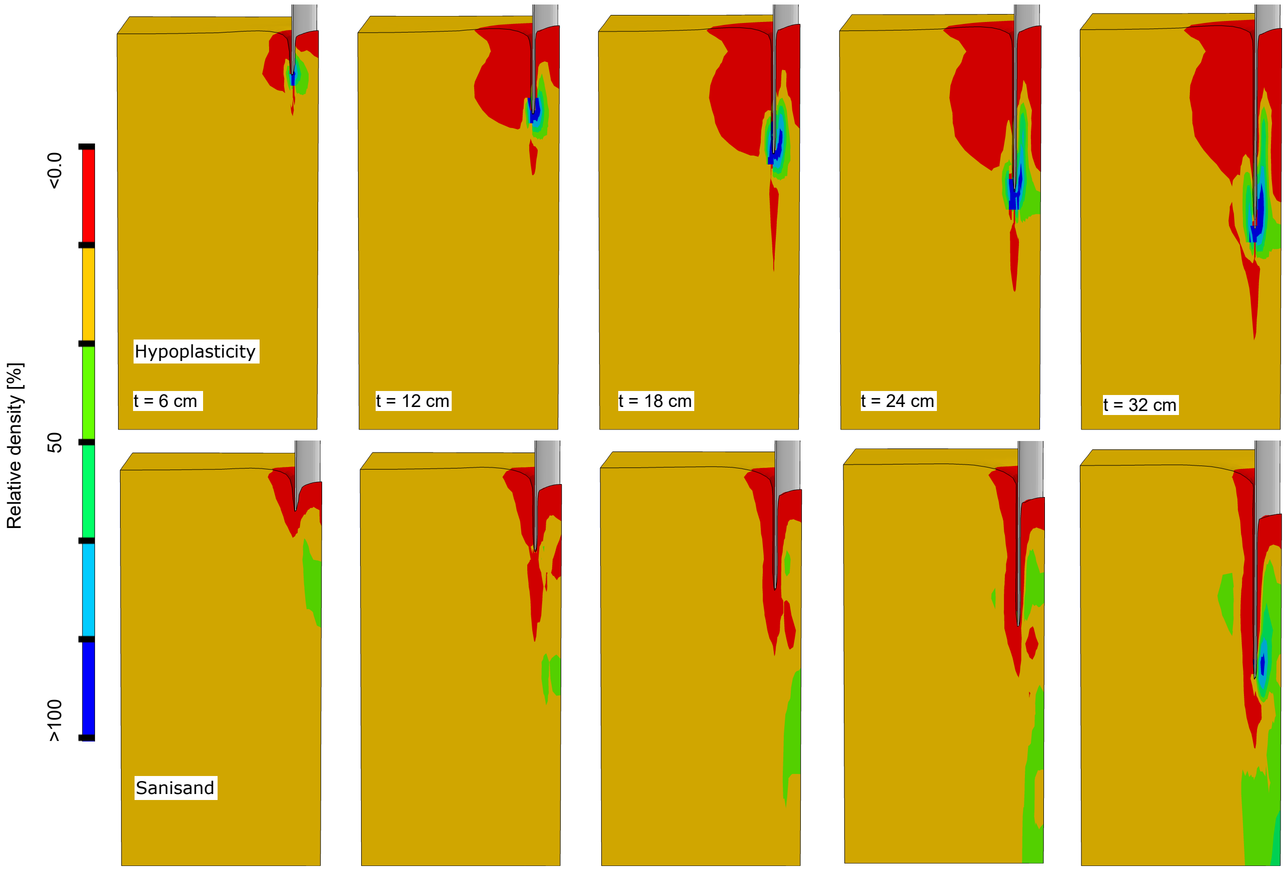

Fig. 6: Spatial distribution of relative density for different pile penetration depths t using the hypoplastic model and Sanisand, respectively.

ground surface. Hence, the plot on the left-hand side displays the radial stress when the pile tip is exactly at the depth at which the stress distribution is evaluated. The plot on the right-hand side shows the radial stress once the pile tip has passed the considered depth by 5 cm. The radial stress distribution for the simulations using the hypoplastic model and Sanisand are displayed. In addition, the initial radial stress is given. The simulations show a large increase in magnitude of radial stress at $t = 25$ cm. The hypoplastic model predicts values larger than $\sigma_r = 100$ kPa in the vicinity of the pile tip. The radial stress decreases strongly with distance to the pile and reaches $\sigma_r = 20$ kPa at the boundary of the model (25 cm from the pile), indicating an influence of the size of the test container on the pile installation process. Compared to the initial radial stress ($\sigma_r \approx 2$ kPa), a considerable increase in radial stress is caused by the pile penetration process. The simulation using Sanisand shows qualitatively a similar increase in radial stress but much lower in magnitude. At the pile tip the radial stress is $\sigma_r \approx 20$ kPa and thus five times lower than the value predicted by the hypoplastic model. With increasing distance to the pile, the radial stress decreases and reaches a value of $\sigma_r \approx 12$ kPa at the model border, which is also lower than the value predicted using the hypoplastic model.

A strong decrease in radial stress close to the pile shaft is observed for both simulations in the plot on the right-hand side of Fig. 8. The simulation using the hypoplastic model predicts a radial stress of $\sigma_r \approx 8$ kPa at the pile shaft whereas in case of Sanisand values close to zero are observed. With increasing distance to the pile shaft, the radial stress increases again, which is more pronounced in case of the hypoplastic model. For distances greater than 10 cm the radial stress remains almost constant for both constitutive models. Much higher values are observed for the hypoplastic model compared to Sanisand, however. Qualitatively, the distributions are again comparable.

The large increase in magnitude of radial stress and the subsequent drop to values lower (for the simulation using Sanisand) in magnitude than the initial radial stress is a mechanism frequently observed in experiments as well (see [56, 24, 6]) and has been described by White & Bolton [56]. Jardine et al. [25] later referred to it as the *cavity expansion-contraction* model. This model can explain the observed changes in the stress distribution around the pile of the present simulations as well. The density of the soil below the pile tip is greatly increased by the pile penetration process in case of the simulation using the hypoplastic model. Once the pile tip passes the heavily densified soil and

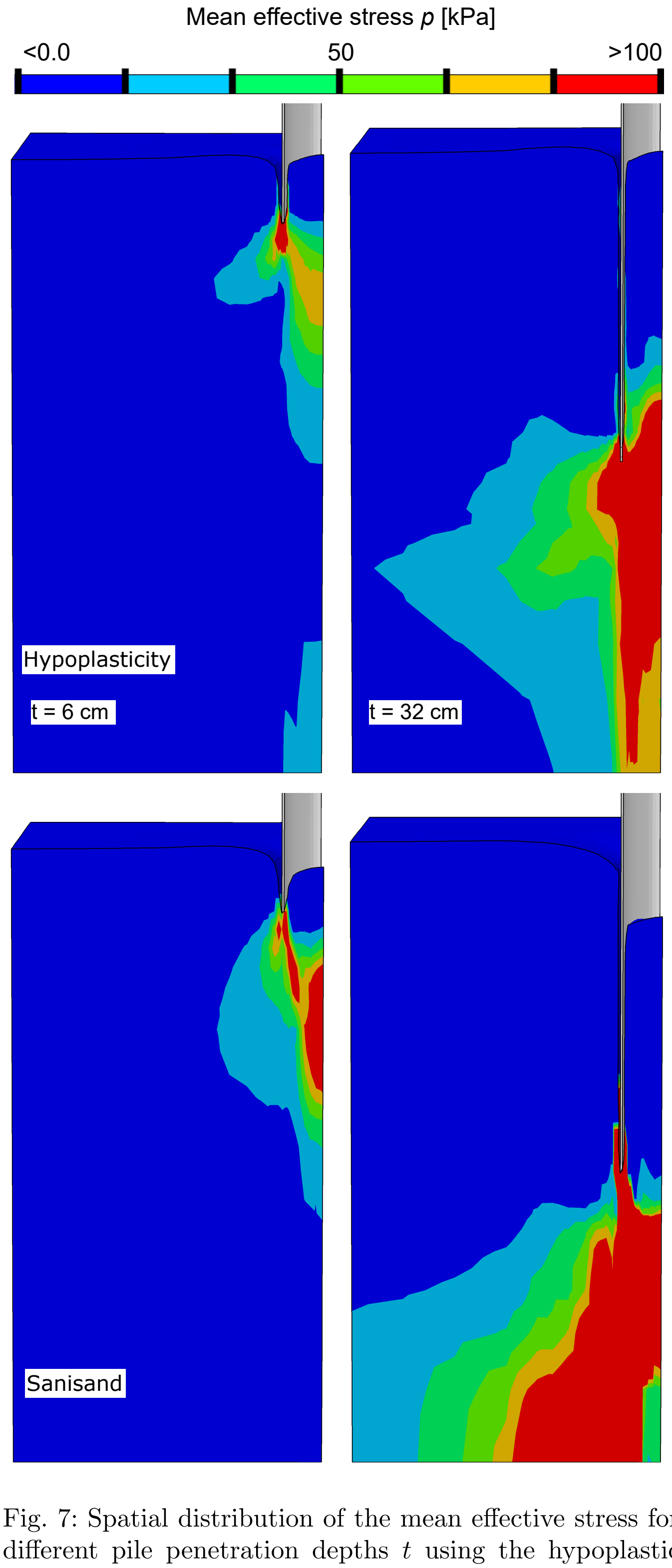

Fig. 7: Spatial distribution of the mean effective stress for different pile penetration depths t using the hypoplastic model and Sanisand, respectively.

the pile-induced stress is reduced, the soil tends to contract under the shearing of the pile shaft. This contraction then reduces the soil stress at the outer shaft even more when the pile penetrates further into the soil.

It is concluded that both constitutive models can reproduce the large increase in magnitude of radial stress and the subsequent drop in magnitude once the pile tip has passed qualitatively. Quantitatively, however, large differences are observed.

5.3 Computational performance

From a computational performance point of view, Sanisand is superior to the hypoplastic model. Using a single processor, the simulation using Sanisand takes approximately 8 hours and 1.3 million increments. The simulation with the hypoplastic model takes close to 20 hours but needs less increments (0.8 million). Hence, the average critical time increment of the (global) explicit time integration scheme using the hypoplastic model is larger than the average critical time increment using Sanisand but the individual increments require more time with the hypoplastic model. It has, however, to be kept in mind that these figures strongly depend on the chosen sub-increment size applied in the implementation of the constitutive models. In terms of numerical stability, i.e. abortion of the simulation due to distortion of elements during the Lagrangian step of the CEL simulation, the constitutive models are found to perform comparable.

6 Simulation of the lateral loading following the pile installation process

Following its installation, the pile was subjected to either monotonic or cyclic lateral loading in the model tests by Leblanc et al. [30]. The simulation of the lateral loading is performed in a purely Lagrangian framework using an implicit solution scheme. The finite element code `numgeo`[1] is used for this purpose. Using `numgeo`, the incorporation of the installation-induced soil changes in the simulation of the lateral loading is more convenient than using `Abaqus`. In terms of results of the simulation of the lateral loading no influence of the finite-element code is expected. This is demonstrated in A by comparison of the results of the two finite-element programs for the simulation of the lateral loading without consideration of the installation process using the hypoplastic model.

6.1 Numerical model

The model used for the lateral loading analysis is displayed in Fig 5b). Reduced integrated, linearly interpolated Lagrangian elements are used. To avoid any hourglassing, an hourglass stiffness of 100 kPa is applied. The state variables of the soil after the installation are transferred to the Lagrangian model using the shortest (euclidean) distance between integration points in the CEL model and in the Lagrangian

[1] `numgeo` (see [35, 38, 36, 50] and `www.numgeo.de`) is an inhouse finite-element program, developed by the first two authors for the solution of non-linear, coupled (dynamic) geotechnical boundary value problems.

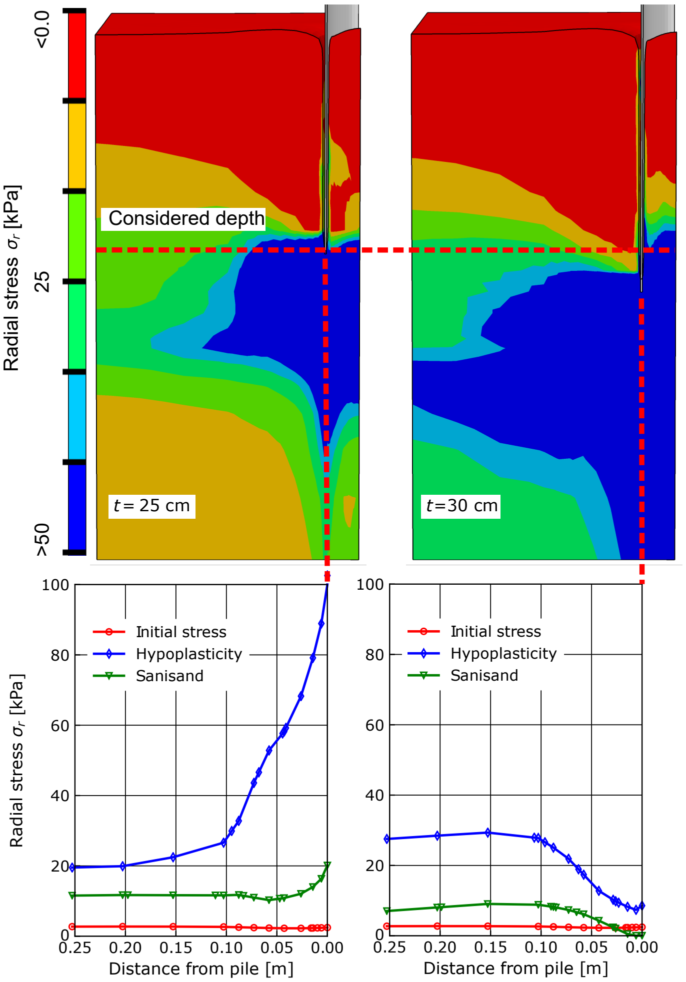

Fig. 8: Top: Distribution of radial stress using the hypoplastic model after a penetration of the pile of 25 cm and 30 cm, respectively. Bottom: Radial stress as function of the radial distance to the pile at a depth of 25 cm below the ground surface using the hypoplastic model and Sanisand. The initial radial stress distribution prior to the driving process is given as well.

model. In addition to stress and void ratio, in case of the hypoplastic model the intergranular strain tensor is considered for the transfer. Note that for the simulations of the lateral loading using Sanisand the distributions resulting from the simulation of the installation using Sanisand are used. Just the same is done for the hypoplastic model. Technically, a "mix", i.e. using the fields after installation of constitutive model A for the lateral loading employing constitutive model B, would be possible as well. Due to the larger number of elements in the Lagrangian model (approximately 50,000), the neighbour search of the closest integration point can take time depending on the implemented scheme. A very fast scheme is obtained using the `SciPy` function `cKDTree` in `Python`. The deformation of the soil caused by the installation process is not considered in the Lagrangian model as the influence of the soil movement is judged insignificant compared to the influence of the change in state variables.

Note that the stress state imported from the CEL model is not resulting in a static force equilibrium. In order to bring the model into equilibrium prior to the lateral loading, an additional calculation step is included allowing the stress to adjust.

6.2 Simulation of the lateral loading

The comparison of the relationships of applied moment (at the ground surface) versus the rotation of the pile from the measurements made in the experiments by Leblanc et al. and the simulation using the hypoplastic model with and without incorporation of the installation-induced soil changes is given in Fig. 9a). Note that for the evaluation of the rotation it is assumed that the pile deforms rigidly above the ground surface. Note in addition that the results of the simulation using the hypoplastic model have already been presented and discussed in [50] (evaluated using non-dimensional values, however). It is evident that the consideration of the installation process leads to a stiffer pile response and a better accordance of the results of the simulation with the measured values. The installation influences the pile response in the range of small rotations stronger than for larger rotations. The final moment after a rotation of $\theta = 0.02$ rad is similar for both simulations.

The simulations using Sanisand are provided in Fig. 9b). The simulation incorporating the installation-induced soil changes does only differ to the wished-in-place simulation after a rotation of $\theta = 0.005$ rad, which is opposite to the observations made for the simulations using the hypoplastic model. With ongoing pile rotation, the moment in the simulation with installation increases stronger than in the simulation without installation. Compared to the experiment, both simulations using Sanisand underestimate the moment resistance and show a worse accordance compared to the simulations using the hypoplastic model.

The differences between the constitutive models found for the lateral loading fit well to the expected tendencies based on the differences observed for the pile installation process. Sanisand predicted less compaction of the soil in the vicinity of the pile tip and much smaller effective radial stresses. It is thus not surprising that the incorporation of the installation induced soil changes leads to a stiffer pile response against lateral loading using the hypoplastic model compared to Sanisand.

The response of the pile to lateral loading in the simulations using Sanisand strongly depends on the parameter G_0, determining the elastic shear stiffness, which is demonstrated in Fig. 10 using $G_0 = 70$ instead of $G_0 = 50$. Note that $G_0 = 50$ has been used for the simulation of the installation process nonethe-

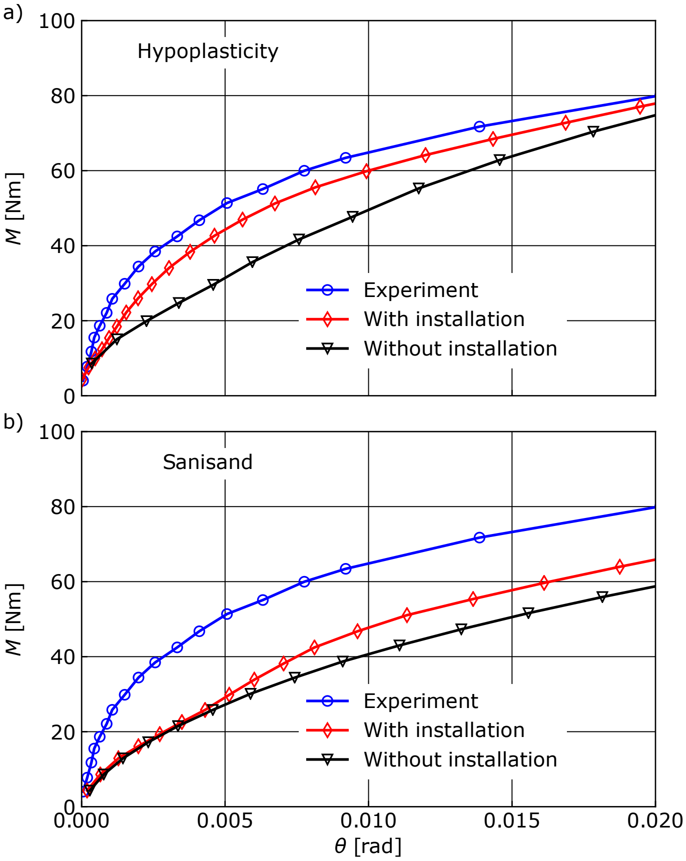

Fig. 9: Applied moment versus resulting rotation of the pile measured in the experiment and obtained from the simulations using the hypoplastic model (a) and Sanisand (b) with and without incorporation of the installation process, respectively

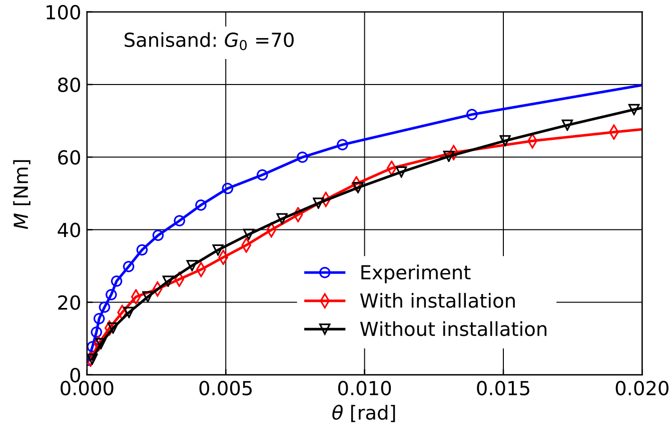

Fig. 10: Applied moment versus resulting rotation of the pile measured in the experiment and obtained from the simulations using Sanisand with and without incorporation of the installation process, respectively. The parameters of Sanisand given in Table 2 with a modification of $G_0 = 70$ have been used.

less. Simulations of the installation using $G_0 = 70$ lead to similar distributions of relative density and stress as presented in Section 5.2 using $G_0 = 50$. It is worth to mention that in the process of the parameter calibration, G_0 does only marginally influence the results of the triaxial tests (within reasonable ranges) and in the present case was determined based on the oedometric compression tests. It has to be clarified, however, that utilizing additional cyclic triaxial tests, a better determination of G_0 based on the measured strain amplitude could have been achieved.

Using $G_0 = 70$ a better accordance of the results of the simulations with the measurements is observed. The influence of the installation, however, is now less pronounced compared to the simulation using $G_0 = 50$. Only marginal differences between the two simulation types, with and without incorporation of the installation process, are visible in Fig. 10.

7 Summary and conclusions

The simulation of small-scale model tests on piles subjected to lateral loading using two constitutive soil models, Sanisand and Hypoplasticity with intergranular strain, has been presented. Prior to the lateral loading, the installation process of the pile has been taken into account. Some aspects of the implementation of the constitutive models in order to achieve a high numerical stability have been discussed. The results of the two constitutive models have been first compared for the simulation of element tests (oedometric compression and drained monotonic triaxial tests) in order to determine the material constants for the yellow Leighton-Buzzard sand used in the model tests. The performance of the constitutive models in case of the triaxial tests was similar whereas the oedometric tests were slightly worse represented using Sanisand. The constitutive models have then been applied for the simulation of pile installation using a Coupled Eulerian-Lagrangian approach. Both constitutive models were found to predict the development of relative density and stress of the soil realistically but large differences in terms of effective radial stress between the models were observed. The simulation using Sanisand showed a much smaller installation-induced increase of effective radial stresses. In terms of computational performance (calculation time), Sanisand was found to be superior to the hypoplastic model.

Following its installation, the pile was subjected to lateral loading and the results of the simulations with and without incorporation of the installation-induced soil changes using the two constitutive models were compared to the measurements made in the experiments by Leblanc et al. [30]. Both constitutive models predicted less rotation of the pile if the installation-induced soil changes were accounted for, which lead to a better accordance with the measurements made in the experiment. The accordance with the experimental data was better in case of the hypoplastic model

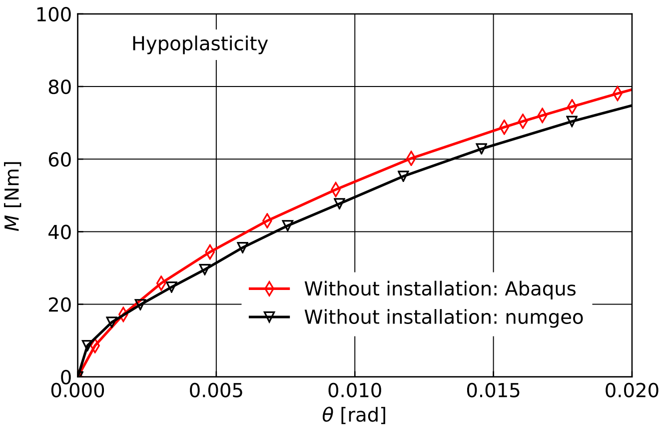

Fig. 11: Applied moment versus resulting rotation of the pile obtained from the simulations using the finite-element codes `numgeo` and `Abaqus`, respectively

compared to Sanisand. In case of the latter constitutive model, the pile response to lateral loading was less influenced by installation effects compared to the simulation using the hypoplastic model. This observation was found to be in accordance with the conclusions drawn from the results regarding the pile installation process, i.e. a smaller increase of effective stress due to the installation process predicted with Sanisand.

It may be concluded that both constitutive models are suitable for the large-deformation analysis of pile installation processes but the results can differ considerably despite a careful calibration with similar performance for the same element test data.

A Comparison of the finite-element code `numgeo` with `Abaqus`

To demonstrate the performance of the in-house finite-element code `numgeo` used to simulate the lateral loading of the pile, a comparison with the proprietary code `Abaqus/Standard` is presented. For that, a simulation without consideration of the installation process and employing the hypoplastic model is performed with both programs. A slightly larger moment resistance is predicted using `Abaqus` compared to `numgeo` for larger pile rotations as is visible from Fig. 11. The differences are, however, judged to be within acceptable range considering the strongly non-linear nature of the boundary value problem at hand.

References

[1] M. Abdelfattah, K. Abdel-Rahman, S. M. Ahmed, and Y. M. El-Mossallamy. "The Role of Constitutive Material Laws on the Jacking of Single Pile Into Sandy Soil Using Coupled Eulerian-Lagrangian Method". In: *Advanced Numerical Methods in Foundation Engineering*. Ed. by H. Shehata, B. Das, A. P. S. Selvadurai, and A. Fayed. Springer International Publishing, 2020, pp. 108–124.

[2] M. Achmus, K. Schmoor, V. Herwig, and B. Matlock. "Lateral bearing behaviour of vibro- and impact-driven large-diameter piles in dense sand". In: *Geotechnik* 43.3 (Aug. 2020), pp. 147–159. DOI: `10.1002/gete.202000006`.

[3] I. Anusic, B. M. Lehane, G. R. Eiksund, and M. A. Liingaard. "Influence of installation method on static lateral response of displacement piles in sand". In: *Geotechnique Letters* 9.3 (2019), pp. 193–197. ISSN: 20452543. DOI: `10.1680/jgele.18.00191`.

[4] M. Bakroon, R. Daryaei, D. Aubram, and F. Rackwitz. "Numerical evaluation of buckling in steel pipe piles during vibratory installation". In: *Soil Dynamics and Earthquake Engineering* 122 (2019), pp. 327–336. ISSN: 0267-7261.

[5] E. Bauer. "Calibration of a comprehensive constitutive equation for granular materials". In: *Soils and Foundations* 36 (1996), pp. 13–26.

[6] F. Burali d'Arezzo, S. Haigh, M. Talesnick, and Y. Ishihara. "Measuring horizontal stresses during jacked pile installation". In: *Proceedings of the Institution of Civil Engineers - Geotechnical Engineering* 168.4 (2015), pp. 306–318.

[7] M. Cecconi, A. DeSimone, C. Tamagnini, and G. M. Viggiani. "A constitutive model for granular materials with grain crushing and its application to a pyroclastic soil". In: *International Journal for Numerical and Analytical Methods in Geomechanics* 26.15 (2002), pp. 1531–1560. ISSN: 03639061. DOI: `10.1002/nag.257`.

[8] Y. F. Dafalias and M. T. Manzari. "Simple Plasticity Sand Model Accounting for Fabric Change Effects". In: *Journal of Engineering Mechanics* 130.6 (2004), pp. 622–634. ISSN: 0733-9399. DOI: `10.1061/(asce)0733-9399(2004)130:6(622)`.

[9] Y. F. Dafalias and M. Taiebat. "SANISAND-Z: zero elastic range sand plasticity model". In: *Géotechnique* 66.12 (2016), pp. 999–1013. DOI: `10.1680/jgeot.15.P.271`.

[10] R. Daryaei, M. Bakroon, D. Aubram, and F. Rackwitz. "Numerical evaluation of the soil behavior during pipe-pile installation using impact and vibratory driving in sand". In: *Soil Dynamics and Earthquake Engineering* 134 (2020), p. 106177. ISSN: 02677261. DOI: `10.1016/j.soildyn.2020.106177`.

[11] J. Dijkstra, W. Broere, and O. M. Heeres. “Numerical simulation of pile installation”. In: *Computers and Geotechnics* 38.5 (2011), pp. 612–622. ISSN: 0266-352X. DOI: https://doi.org/10.1016/j.compgeo.2011.04.004.

[12] G. J. Dyson and M. F. Randolph. “Monotonic Lateral Loading of Piles in Calcareous Sand”. In: *Journal of Geotechnical and Geoenvironmental Engineering* 127.4 (2001), pp. 346–352. DOI: 10.1061/(ASCE)1090-0241(2001)127:4(346).

[13] S. Fan, B. Bienen, and M. F. Randolph. “Effects of Monopile Installation on Subsequent Lateral Response in Sand. II: Lateral Loading”. In: *Journal of Geotechnical and Geoenvironmental Engineering* 147.5 (May 2021), p. 04021022. ISSN: 1090-0241. DOI: 10.1061/(ASCE)GT.1943-5606.0002504.

[14] S. Fan, B. Bienen, and M. F. Randolph. “Centrifuge study on effect of installation method on lateral response of monopiles in sand”. In: *International Journal of Physical Modelling in Geotechnics* 21.1 (2021), pp. 40–52. ISSN: 20426550. DOI: 10.1680/jphmg.19.00013.

[15] S. Fan, B. Bienen, and M. F. Randolph. “Effects of Monopile Installation on Subsequent Lateral Response in Sand. I: Pile Installation”. In: *Journal of Geotechnical and Geoenvironmental Engineering* 147.5 (2021), p. 04021021. ISSN: 1090-0241. DOI: 10.1061/(asce)gt.1943-5606.0002467.

[16] J. Grabe and E. Heins. “Coupled deformation-seepage analysis of dynamic capacity tests on open-ended piles in saturated sand”. In: *Acta geotechnica* 12.1 (2016), pp. 211–223. ISSN: 1861-1133.

[17] F. Hamad. “Formulation of the axisymmetric CPDI with application to pile driving in sand”. In: *Computers and Geotechnics* 74 (2016), pp. 141–150. ISSN: 18737633. DOI: 10.1016/j.compgeo.2016.01.003.

[18] T. Hamann, G. Qiu, and J. Grabe. “Application of a Coupled Eulerian-Lagrangian approach on pile installation problems under partially drained conditions”. In: *Computers and Geotechnics* 63 (2015), pp. 279–290. ISSN: 0266-352X. DOI: https://doi.org/10.1016/j.compgeo.2014.10.006.

[19] T. Hamann, G. Qiu, and J. Grabe. “Application of a Coupled Eulerian–Lagrangian approach on pile installation problems under partially drained conditions”. In: *Computers and Geotechnics* 63 (Jan. 2015), pp. 279–290. DOI: 10.1016/j.compgeo.2014.10.006.

[20] E. Heins and J. Grabe. “Class-A-prediction of lateral pile deformation with respect to vibratory and impact pile driving”. In: *Computers and Geotechnics* 86 (2017), pp. 108–119. ISSN: 18737633. DOI: 10.1016/j.compgeo.2017.01.007.

[21] S. Henke and J. Grabe. “Numerical investigation of soil plugging inside open-ended piles with respect to the installation method”. In: *Acta Geotechnica* 3.3 (2008), pp. 215–223.

[22] B. Hoffmann, J. Labenski, and C. Moormann. “Effects of Vibratory Driving of Monopiles on Soil Conditions and Their Cyclic Lateral Load Bearing Behavior”. In: *4th International Symposium on Frontiers in Offshore Geotechnics*. Vol. 49. 0. 2020, pp. 714–724.

[23] A. F. Homayoun Rooz and A. Hamidi. “A numerical model for continuous impact pile driving using ALE adaptive mesh method”. In: *Soil Dynamics and Earthquake Engineering* 118 (2019), pp. 134–143. ISSN: 02677261. DOI: 10.1016/j.soildyn.2018.12.014.

[24] R. J. Jardine, B. T. Zhu, P. Foray, and Z. X. Yang. “Measurement of stresses around closed-ended displacement piles in sand”. In: *Géotechnique* 63.1 (2013), pp. 1–17. DOI: 10.1680/geot.9.P.137.

[25] R. J. Jardine, B. T. Zhu, P. Foray, and Z. X. Yang. “Interpretation of stress measurements made around closed-ended displacement piles in sand”. In: *Geotechnique* 63.8 (2013), pp. 613–627. ISSN: 00168505. DOI: 10.1680/geot.9.P.138.

[26] R. T. Klinkvort. “Centrifuge modelling of drained lateral pile - soil response: Application for offshore wind turbine support structures”. PhD thesis. 2013. ISBN: 9788778773579.

[27] J. Labenski, C. Moormann, J. Aschrafi, and B. Bienen. “Simulation of the plug inside open steel pipe piles with regards to different installation methods”. In: *Proceedings of 13th Baltic Sea Geotechnical Conference*. Vilnius Gediminas Technical University, Vilnius, Lithuania. 2016, pp. 223–230.

[28] A. Lashkari. “A SANISAND model with anisotropic elasticity”. In: *Soil Dynamics and Earthquake Engineering* 30.12 (2010), pp. 1462–1477. ISSN: 0267-7261. DOI: https://doi.org/10.1016/j.soildyn.2010.06.015.

[29] V. H. Le, F. Remspecher, and F. Rackwitz. "Development of numerical models for the long-term behaviour of monopile foundations under cyclic loading considering the installation effects". In: *Soil Dynamics and Earthquake Engineering* 150 (2021), p. 106927. ISSN: 02677261. DOI: 10.1016/j.soildyn.2021.106927.

[30] C. Leblanc, G. T. Houlsby, and B. W. Byrne. "Response of stiff piles in sand to long-term cyclic lateral loading". In: *Géotechnique* 60.2 (2010), pp. 79–90.

[31] L. Li, W. Wu, M. Hesham El Naggar, G. Mei, and R. Liang. "DEM analysis of the sand plug behavior during the installation process of open-ended pile". In: *Computers and Geotechnics* 109 (2019), pp. 23–33. ISSN: 0266-352X. DOI: https://doi.org/10.1016/j.compgeo.2019.01.014.

[32] H. Y. Liu, J. A. Abell, A. Diambra, and F. Pisano. "Modelling the cyclic ratcheting of sands through memory-enhanced bounding surface plasticity". In: *Géotechnique* 69.9 (2019), pp. 783–800. DOI: 10.1680/jgeot.17.P.307.

[33] H. Y. Liu and F. Pisano. "Prediction of oedometer terminal densities through a memory-enhanced cyclic model for sand". In: *Geotechnique Letters* 9.2 (2019), pp. 81–88. DOI: 10.1680/jgele.18.00187.

[34] J. Liu, N. Duan, L. Cui, and N. Zhu. "DEM investigation of installation responses of jacked open-ended piles". In: *Acta Geotechnica* 14.6 (2019), pp. 1805–1819.

[35] J. Machaček and P. Staubach. "numgeo: A finite-element program for the simulation of hydro-mechanically coupled geotechnical processes". In: *Fachsektionstage Geotechnik 2021*. DGGT, 2021.

[36] J. Machaček, P. Staubach, M. Tafili, H. Zachert, and T. Wichtmann. "Investigation of three sophisticated constitutive soil models: From numerical formulations to element tests and the analysis of vibratory pile driving tests". In: *Computers and Geotechnics* 138 (2021), p. 104276. ISSN: 18737633. DOI: 10.1016/j.compgeo.2021.104276.

[37] J. Machaček, T. Triantafyllidis, and P. Staubach. "Fully coupled simulation of an opencast mine subjected to earthquake loading". In: *Soil Dynamics and Earthquake Engineering* 115 (2018), pp. 853–867. ISSN: 02677261. DOI: 10.1016/j.soildyn.2018.09.016.

[38] J. Machaček. "Contributions to the numerical modeling of saturated and unsaturated soils". PhD thesis. Institut für Bodenmechanik und Felsmechanik am Karlsruher Institut für Technologie (KIT), 2020.

[39] H. Matsuoka and T. Nakai. "A new failure criterion for soils in three-dimensional stresses". In: *Deformation and Failure of Granular Materials*. 1982, pp. 253–263.

[40] A. Niemunis and I. Herle. "Hypoplastic model for cohesionless soils with elastic strain range". In: *Mechanics of Cohesive-Frictional Materials* 2.4 (1997), pp. 279–299. ISSN: 10825010. DOI: 10.1002/(SICI)1099-1484(199710)2:4<279::AID-CFM29>3.0.CO;2-8.

[41] V. A. Osinov, S. Chrisopoulos, and C. Grandas-Tavera. "Vibration-induced stress changes in saturated soil: A high-cycle problem". In: *Lecture Notes in Applied and Computational Mechanics*. Vol. 80. 2016, pp. 69–84. ISBN: 978-3-319-23158-7. DOI: 10.1007/978-3-319-23159-4_4.

[42] A. L. Petalas, Y. F. Dafalias, and A. G. Papadimitriou. "SANISAND-F: Sand constitutive model with evolving fabric anisotropy". In: *International Journal of Solids and Structures* 188-189 (2020), pp. 12–31. ISSN: 00207683. DOI: 10.1016/j.ijsolstr.2019.09.005.

[43] N. T. V. Phuong, A. F. van Tol, A. S. K. Elkadi, and A. Rohe. "Numerical investigation of pile installation effects in sand using material point method". In: *Computers and Geotechnics* 73 (2016), pp. 58–71. ISSN: 0266-352X. DOI: https://doi.org/10.1016/j.compgeo.2015.11.012.

[44] N. T. Phuong, A. Rohe, R. B. Brinkgreve, and A. F. van Tol. "Hypoplastic model for crushable sand". In: *Soils and Foundations* 58.3 (2018), pp. 615–626. ISSN: 00380806. DOI: 10.1016/j.sandf.2018.02.022.

[45] T. Pucker and J. Grabe. "Numerical simulation of the installation process of full displacement piles". In: *Computers and Geotechnics* 45 (2012), pp. 93–106. ISSN: 0266352X. DOI: 10.1016/j.compgeo.2012.05.006.

[46] G. Qiu, S. Henke, and J. Grabe. "Application of a Coupled Eulerian-Lagrangian Approach on Geomechanical Problems Involving Large Deformation". In: *Computers and Geotechnics* 38 (2011), pp. 30–39.

[47] S. W. Sloan. "Substepping schemes for the numerical integration of elastoplastic stress-strain relations". In: *International Journal for Numerical Methods in Engineering* 24.5 (1987), pp. 893–911. DOI: https://doi.org/10.1002/nme.1620240505.

[48] M. Soleimani and C. Weissenfels. "Numerical simulation of pile installations in a hypoplastic framework using an SPH based method". In: *Computers and Geotechnics* 133 (2021), p. 104006. ISSN: 0266-352X. DOI: https://doi.org/10.1016/j.compgeo.2021.104006.

[49] P. Staubach and J. Machaček. "Influence of relative acceleration in saturated sand: Analytical approach and simulation of vibratory pile driving tests". In: *Computers and Geotechnics* 112 (Aug. 2019), pp. 173–184. ISSN: 0266352X. DOI: 10.1016/j.compgeo.2019.03.027.

[50] P. Staubach, J. Machaček, R. Sharif, and T. Wichtmann. "Back-analysis of model tests on piles in sand subjected to long-term lateral cyclic loading: Impact of the pile installation and application of the HCA model". In: *Computers and Geotechnics* 134 (June 2021), p. 104018. ISSN: 0266352X. DOI: 10.1016/j.compgeo.2021.104018.

[51] P. Staubach, J. Machaček, and T. Wichtmann. "Impact of the installation on the long-term behaviour of offshore wind turbine pile foundations". In: *4th International Symposium on Frontiers in Offshore Geotechnics,* Taylor & Francis Group, London, UK, 2020, pp. 573–583.

[52] P. Staubach, J. Machaček, M. C. Moscoso, and T. Wichtmann. "Impact of the installation on the long-term cyclic behaviour of piles in sand: A numerical study". In: *Soil Dynamics and Earthquake Engineering* 138 (2020), p. 106223. ISSN: 02677261. DOI: 10.1016/j.soildyn.2020.106223.

[53] P. Staubach, J. Machaček, J. Skowronek, and T. Wichtmann. "Vibratory pile driving in water-saturated sand: Back-analysis of model tests using a hydro-mechanically coupled CEL method". In: *Soils and Foundations* 61.1 (Feb. 2021), pp. 144–159. ISSN: 00380806. DOI: 10.1016/j.sandf.2020.11.005.

[54] M. Taiebat and Y. Dafalias. "SANISAND, simple anisotropic sand plasticity model". In: *International Journal For Numerical And Analytical Methods in Geomechanics* 32.8 (2008), pp. 915–948.

[55] D. Wang, B. Bienen, M. Nazem, Y. Tian, J. Zheng, T. Pucker, and M. F. Randolph. "Large deformation finite element analyses in geotechnical engineering". In: *Computers and Geotechnics* 65 (Apr. 2015), pp. 104–114. DOI: 10.1016/j.compgeo.2014.12.005.

[56] D. J. White and B. M. Lehane. "Friction fatigue on displacement piles in sand". In: *Geotechnique* 54.10 (2004), pp. 645–658. ISSN: 00168505. DOI: 10.1680/geot.2004.54.10.645.

[57] T. Wichtmann, W. Fuentes, and T. Triantafyllidis. "Inspection of three sophisticated constitutive models based on monotonic and cyclic tests on fine sand: Hypoplasticity vs. Sanisand vs. ISA". In: *Soil Dynamics and Earthquake Engineering* 124 (2019), pp. 172–183. ISSN: 0267-7261. DOI: https://doi.org/10.1016/j.soildyn.2019.05.001.

[58] P.-A. von Wolffersdorff. "A hypoplastic relation for granular materials with a predefined limit state surface". In: *Mechanics of Cohesive-Frictional Materials* 1 (1996), pp. 251–271.

[59] M. Yang, M. Taiebat, and Y. F. Dafalias. "SANISAND-MSf: a sand plasticity model with memory surface and semifluidised state". In: *Géotechnique* (Dec. 2020), pp. 1–20. ISSN: 0016-8505. DOI: 10.1680/jgeot.19.P.363.

[60] Z. X. Yang, Y. Y. Gao, R. J. Jardine, W. B. Guo, and D. Wang. "Large Deformation Finite-Element Simulation of Displacement-Pile Installation Experiments in Sand". In: *Journal of Geotechnical and Geoenvironmental Engineering* 146.6 (2020), p. 4020044. DOI: 10.1061/(ASCE)GT.1943-5606.0002271.